JBMR Plus, 2025, **9**, ziae133
https://doi.org/10.1093/jbmrpl/ziae133
Advance access publication: October 23, 2024
Research Article

Geranylgeranyl diphosphate synthase inhibition impairs osteoclast differentiation, morphology, and resorptive activity

Molly E. Muehlebach[1], Staci L. Haney[2], Yashpal S. Chhonker[3], Mamunur Rashid[3], Daryl J. Murry[3], Geoffrey Talmon[4], Sarah A. Holstein[2,*]

[1]Cancer Research Doctoral Program, University of Nebraska Medical Center, Omaha, NE 68198, United States
[2]Department of Internal Medicine, University of Nebraska Medical Center, Omaha, NE 68198, United States
[3]Department of Pharmacy Practice and Science, University of Nebraska Medical Center, Omaha, NE 68198, United States
[4]Department of Pathology and Microbiology, University of Nebraska Medical Center, Omaha, NE 68198, United States

*Corresponding author: Sarah A. Holstein, Division of Oncology and Hematology, Department of Internal Medicine, University of Nebraska Medical Center, Omaha, NE 68198, United States (sarah.holstein@unmc.edu)

Abstract

Nitrogen bisphosphonates, such as zoledronic acid, target the enzyme farnesyl diphosphate synthase (FDPS) in the isoprenoid biosynthetic pathway (IBP), and are the frontline treatment for osteolytic bone diseases. A strong affinity of these agents for bone limits their distribution out of the skeleton. Geranylgeranyl diphosphate synthase (GGDPS) is directly downstream to FDPS in the IBP and novel GGDPS inhibitors such as RAM2061 have been shown to have key drug-like features including prolonged half-life, metabolic stability, and systemic distribution. Furthermore, RAM2061 exerts anti-neoplastic benefits in mouse models of multiple myeloma and Ewing sarcoma. Therefore, we are interested in determining the potential impact of RAM2061 on osteoclast biology and bone remodeling. Studies utilizing undifferentiated RAW264.7 cells demonstrated that treatment with RAM2061 depletes cells of geranylgeranyl diphosphate, impairs protein geranylgeranylation, and induces markers of the unfolded protein response pathway and apoptosis. Differentiation of RAW264.7 cells to mature osteoclasts is disrupted by RAM2061, resulting in decreased numbers of mature osteoclasts, altered morphology, and decreased tartrate-resistant acid phosphatase activity. Treatment of fully differentiated RAW264.7 cells with RAM2061 led to decreased resorptive activity. Confocal microscopy studies revealed that RAM2061 disrupts Cdc42 localization, inhibiting proper actin ring formation in osteoclasts. No significant impact on bone turnover markers or bone histomorphology was observed following a 3-week treatment of CD-1 mice with RAM2061, although decreased numbers of osteoclasts were observed. Liquid chromatography-tandem mass spectrometry studies confirmed accumulation of RAM2061 in bone from the in vivo studies as well as hydroxyapatite binding in vitro. In conclusion, these studies are the first to demonstrate the anti-osteoclastic activity of GGDPS inhibitor treatment and support future studies exploring the therapeutic benefit of this novel therapy in the setting of pathological bone remodeling.

Keywords: osteoclasts, antiresorptives, molecular pathways—remodeling, preclinical studies, other (therapeutics)

Lay Summary

Nitrogen bisphosphonates (NBPs) are the frontline treatment for bone diseases characterized by excessive bone loss. Laboratory studies have suggested NBPs have anti-cancer effects as well, but due to these agents very strongly binding to bone, significant anti-cancer activity has not been observed in animal or human studies. Our novel drug (RAM2061) targets an enzyme called geranylgeranyl diphosphate synthase that is closely related to the target of the clinically used NBPs and shares some structural similarities. However, our prior studies have shown that RAM2061 does penetrate tissues throughout the body and has anti-tumor activity in a variety of mouse models of cancer, including multiple myeloma, which is a cancer associated with bone destruction. In this study we investigate whether RAM2061 has any direct effects on the bone cells (osteoclasts) that control bone resorption. These studies reveal that RAM2061 impacts the cellular growth and differentiation of osteoclasts as well as impairs their resorptive ability. Mouse studies using normal, young mice were performed in which animals were treated with RAM2061 for 3 weeks. These studies demonstrated accumulation of RAM2061 in the bone, as well as a decrease in osteoclast number, but did not show a significant impact on bone turnover markers or bone volume. These studies are the first to show that this novel treatment impacts osteoclast activity as well as accumulate in the bones and form the basis for future studies exploring the effects of RAM2061 in mouse models of bone disease.

Received: July 17, 2024. **Revised:** October 15, 2024. **Accepted:** October 21, 2024

Graphical Abstract

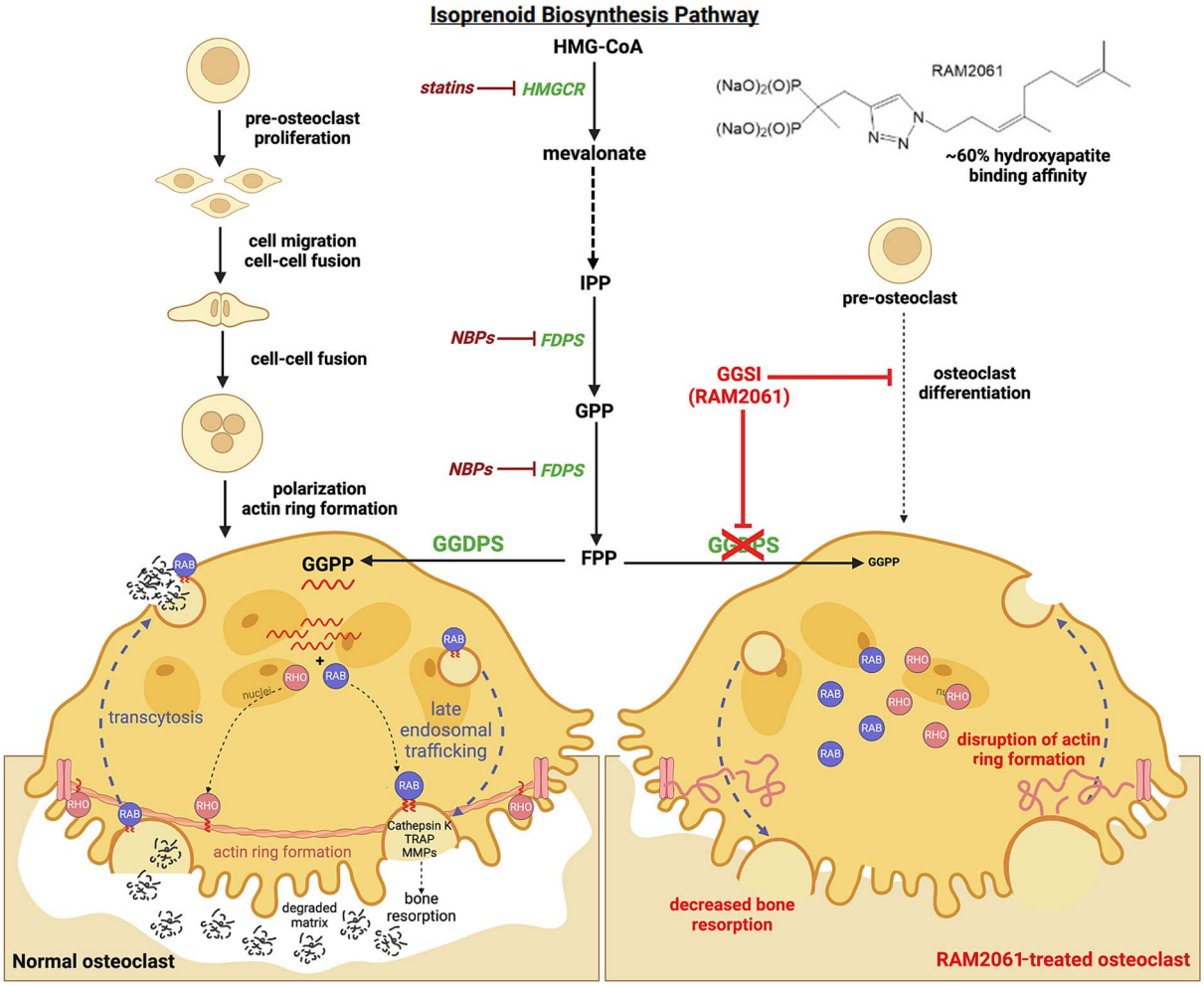

Introduction

The isoprenoid biosynthesis pathway (IBP) is currently targeted clinically by 2 major classes of drugs: the statins (cholesterol lowering agents) and nitrogen bisphosphonates (NBPs, bone targeting agents). The pathway is responsible for the production of the 15-carbon farnesyl pyrophosphate (FPP) and 20-carbon geranylgeranyl diphosphate (GGPP), which serve as substrates for the posttranslational modification (prenylation) of small GTPases in the Ras, Rab, and Rho subfamilies. When prenylation is impaired, these proteins cannot localize or function properly.[1] With Ras, Rab, and Rho proteins all serving essential roles in cellular function, inhibiting production of these isoprenoid donors can impact cell activity and survival.[2,3]

NBPs, such as zoledronic acid (ZA), inhibit the enzyme farnesyl diphosphate synthase (FDPS), which is responsible for the production of FPP that is utilized for the farnesylation of Ras proteins. FPP is also utilized by the enzyme geranylgeranyl diphosphate synthase (GGDPS) for production of GGPP, which serves as the substrate for geranylgeranylation of proteins in the Rab and Rho subfamilies. The bisphosphonate moiety of NBPs contains a phosphorous-carbon-phosphorous (P-C-P) backbone that facilitates chelation of calcium ions, conferring a strong affinity for binding hydroxyapatite (HAP) crystals in bone. This promotes NBPs accumulation in the bone matrix where they are endocytosed by osteoclasts during bone resorption and induce apoptosis.[4] NBPs have an overall bone-strengthening benefit in skeletal diseases that are characterized by excessive osteoclast-mediated resorption, exemplified by their efficacy in reducing skeletal morbidity in a variety of osteoresorptive and metastatic bone diseases.[5–7] In vitro studies have suggested additional anti-neoplastic properties; however this has yet to be replicated in vivo due to lack of systemic distribution, with ZA primarily accumulating in the bone and remaining drug cleared unmodified through the kidneys.[8–12]

Of note, the anti-resorptive effects of NBPs in osteoclasts are attributed to depletion of intracellular GGPP, independent of FPP depletion.[6,13] This is due to the essential role of geranylgeranylated Rho proteins in cytoskeletal rearrangement necessary for proper osteoclast differentiation and resorption.[14] As intracellular depletion of GGPP is the primary mechanism of NBPs anti-osteoclastic effects, selective inhibition of GGDPS itself would provide a more targeted approach without potential off-target effects from FDPS inhibition, such as FPP depletion and disruption of cholesterol biosynthesis.

GGDPS inhibitors (GGSIs) are under investigation as potential anti-cancer agents, with specific focus on malignancies characterized by aberrant protein production.[15–17] We have focused on the development of a class of novel GGSIs that are

isoprenoid triazole bisphosphonates.[15,18–20] From extensive structure-function studies, a lead GGSI, named RAM2061 (α-methyl homoneryl triazole bisphosphonate), was identified, with key drug-like features (prolonged half-life and systemic distribution) and anti-tumor effects in vivo.[15–17,21–23] From these studies we found GGDPS inhibition to represent a novel therapeutic approach by targeting protein trafficking leading to ER-stress induced apoptosis.[16,17,24] For example, in multiple myeloma cells, RAM2061 disrupts intracellular monoclonal protein trafficking as a consequence of inhibition of Rab protein geranylgeranylation, leading to induction of the unfolded protein response (UPR) pathway and apoptosis.[24]

While previous efforts have focused on the direct anti-cancer effects of RAM2061 and other GGSIs, we were interested in determining whether this novel drug strategy has a direct impact on osteoclast function and bone biology. In this study we found that RAM2061 demonstrates direct anti-osteoclastic effects through inhibition of protein geranylgeranylation and disruption of cytoskeletal processes necessary for proper differentiation and function in vitro. To replicate the physiological setting of normal bone remodeling, we utilized outbred female CD-1 mice at 6-8 weeks of age. In vivo evaluation of limited duration RAM2061 treatment did not substantially alter bone morphology, but did decrease osteoclast numbers. This work supports the need for future studies to determine the impact of RAM2061 on osteolytic diseases such as myeloma bone disease (MBD).

Materials and methods

Chemicals

Dr. David Wiemer (University of Iowa) provided RAM2061. Compound purity was determined as ≥95% by high-performance liquid chromatography and verified by nuclear magnetic resonance.[20] Zoledronic acid was obtained from Pfizer. Compound structures are shown in Figure 1A. Lovastatin and GGPP were obtained from Sigma-Aldrich.

Cell lines

RAW264.7 cells (ATCC) were grown in DMEM high glucose media with L-glutamine supplemented with 10% heat-inactivated fetal bovine serum (FBS) and 1% penicillin-streptomycin at 37 °C and 5% CO_2.

HAP binding affinity

A 1 mg/mL HAP slurry was prepared in 0.05 M Tris-HCl buffer. HAP suspension (0.8 mL) and RAM2061 (1 or 10 μM) were added to an Eppendorf tube, while calibration standards (0.14-500 ng/mL) and quality controls (lower limit of quantification [0.13 ng/mL]), low quality control (0.5 ng/mL), middle quality control (125 ng/mL), and high-quality control (375 ng/mL) were prepared simultaneously. Samples were shaken at room temperature (RT) for 1 h to allow for compound binding. Following incubation, tubes were spun down, and supernatant was collected to quantify residual abundance of drug. Internal standard (IS; RAM1147 1 μg/mL) was added to all samples.[25] RAM2061 samples (100 μL) were diluted in ammonium carbonate buffer (10 mM, 400 μL) with 0.1% NH_4OH in duplicate. Solid phase extraction (SPE) and liquid chromatography with tandem mass spectrometry (LC-MS/MS) were conducted following the workflow described below for bone homogenate samples.

Intracellular FPP/GGPP analysis

Intracellular concentrations of FPP and GGPP were quantified using a validated LC-MS/MS methodology as previously described.[26] RAW264.7 cells were seeded (2×10^5 cells/well) in 6-well plates and incubated in the presence or absence of RAM2061 or ZA. Following 48 h treatment, cells were counted using trypan blue staining and a Bio-Rad TC20 automated cell counter. Cells were pelleted, washed in PBS, and stored at −20 °C prior to processing by SPE for LC-MS/MS analysis. Isoprenoid concentrations were normalized to total number of viable cells. Samples in which levels of GGPP were below the limit of quantitation (≥0.04 ng/mL) were reported as ND (not detected).

MTT cytotoxicity assay

Cells were seeded (5×10^3 cells/well) in 96-well flat-bottom plates and incubated in the presence or absence of RAM2061. Following 24, 48, or 72 h incubation, 35 μL of a MTT (3-(4,5-dimethylthiazol-2-yl)-2,5-diphenyl 2) solution (5 mg/mL in PBS) was added to each well. Following incubation at 37 °C for 4 h, 100 μL of solubilizing solution (0.01 M HCl/10% SDS) was added and plates were left to shake at 37 °C overnight. Absorbance was measured using a 2017 Tecan microplate spectrophotometer. Data were normalized to solvent-treated control wells defined as having an MTT activity of 100%.

Immunoblot

RAW264.7 cells were incubated in the presence or absence of RAM2061, or in some studies incubated with either lovastatin, ZA, or GGPP. Following specified time periods, cells were washed in PBS and lysed using RIPA buffer (1% sodium deoxycholate, 0.15 M NaCl, 0.1% SDS, 1% (v/v) Triton-X-100, 0.05 M Tris HCl, pH 7.4) supplemented with protease and phosphatase inhibitors to generate whole cell lysate. Protein content was determined using the BCA method. Protein (15 μg) was loaded on an SDS-PAGE gel and transferred to polyvinylidene difluoride membrane.

Mandible and long bones from CD-1 mice were homogenized in 15% EDTA solution using a TissueLyserII (Qiagen) and 3 mm tungsten carbide beads (Qiagen). An aliquot of bone homogenate (100 μL) was lysed 1:1 in T-PER (Invitrogen) supplemented with protease inhibitors using a hand-held tissue homogenizer. Lysed homogenate (30 μL) was supplemented with 6x Laemmli buffer and heated at 95 °C for 10 min. Samples were loaded on an SDS-PAGE gel and transferred to a polyvinylidene difluoride membrane.

Blots were incubated overnight at 4 °C in primary antibody and for 1 h RT in secondary antibody. Blots were imaged using Bio-Rad Chemidoc MP imaging system following addition of ECL chemiluminescence reagent.

Information regarding the antibodies used in the immunoblotting experiments can be found in Supplemental Materials (Table S1).

Quantitative real-time polymerase chain reaction

Cells were seeded (2×10^5 cells/well) in 6-well flat-bottom plates and incubated in the presence or absence of RAM2061 or ZA. Subsequently, RNA extraction was performed using Omega Bio-Tek EZNA RNA total isolation kit. RNA content

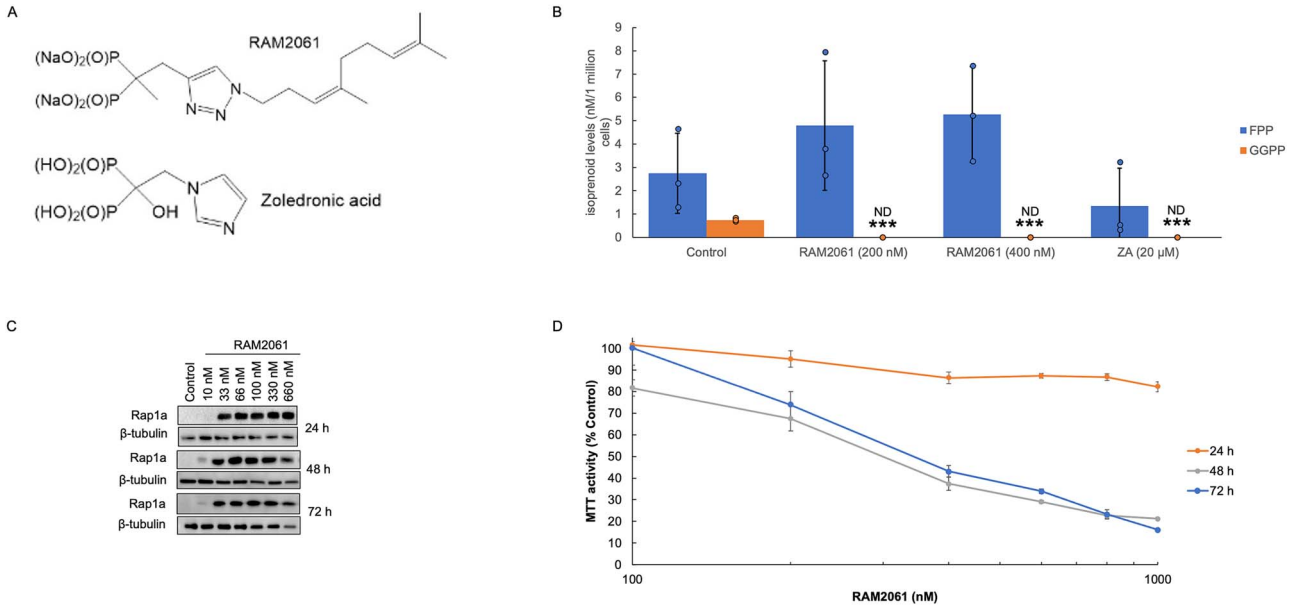

Figure 1. RAM2061 demonstrates on-target activity and cytotoxic effects in undifferentiated RAW264.7 cells. (A) RAM2061 and zoledronic acid chemical structures. (B) Levels of intracellular farnesyl pyrophosphate (FPP) and geranylgeranyl diphosphate (GGPP) in RAW264.7 cells following 48 h incubation in the presence or absence of RAM2061 (200 or 400 nM) or zoledronic acid (ZA, 20 μM) ($n = 3$ biological replicates, data are displayed as mean ± SD; ND = not detected; *** denotes $p < .001$ per t-test). (C) Immunoblot analysis for unmodified Rap1a (Rap1a) and β-tubulin (loading control) following 24, 48, or 72 h incubation with varying concentrations of RAM2061 in RAW264.7 cells. Immunoblots are representative of 3 independent experiments. (D) MTT assays were performed following a 24, 48, or 72 h incubation period with RAM2061 in RAW264.7 cells ($n = 4$, data are displayed as mean ± SD).

and purity was measured using a Nanodrop spectrophotometer. Complementary DNA (cDNA) was prepared using the iScript cDNA synthesis kit (Bio-Rad). iTaq Universal SYBR Green Supermix (Bio-Rad) was mixed with cDNA and gene specific primers according to manufacturer's instructions. Quantitative real-time polymerase chain reactions (qRT-PCR) were performed in triplicate using a Bio-Rad CFX96 real time machine. Bio-Rad CFX manager 3.1 software was used for data analysis and gene expression was normalized to housekeeping gene $\beta 2$ microglobulin (B2M). Primer sequences can be found in Supplemental Materials (Table S2).

XBP1 splicing

Following incubation of cells in the presence or absence of RAM2061, RNA extraction was performed as described above and cDNA was prepared. PCR was performed using XBP1- specific primers (Supplemental Materials). PCR products were separated on a 2% agarose gel, stained with ethidium bromide, and visualized using a Bio-Rad Chemidoc MP imaging system.

Osteoclast differentiation

RAW264.7 cells were cultured in MEM alpha (1x) media without phenol red and supplemented with 10% heat-inactivated FBS and 1% penicillin-streptomycin at 37 °C and 5% CO_2. Cells were plated at 3.125×10^3 cells/cm^2 and treated with 30 ng/mL macrophage colony stimulating factor (M-CSF) (R&D). Cells were then treated with 40 ng/mL receptor activator of nuclear-κB ligand (RANKL) (R&D) consecutively for 4 days to attain mature osteoclasts.

Tartrate-resistant acid phosphatase staining

RAW265.7 cells were differentiated in a 96-well plate until the designated time point. For the analysis of secreted tartrate-resistant acid phosphatase (TRAP) activity, 30 μL of cell culture media was collected and incubated with 170 μL of tartrate buffer mixed with chromogenic substrate supplied by the Cosmo Bio. Co. LTD TRAP staining kit. Following 3 h incubation at 37 °C, absorbance was measured at 540 nm and normalized to control wells. For the identification of TRAP+ osteoclasts, cells were fixed at their designated time point during the differentiation period and stained in 50 μL of the tartrate buffer with chromogenic substrate for 1 h at 37 °C. Following incubation, cells were washed and imaged using an EVOS cell imaging microscope at 20x.

Bone resorption assay

RAW264.7 cells were plated 2.5×10^3 on 48-well bone resorption plates obtained from Cosmo Bio. Co. LTD. Cells were differentiated over the span of 4 days. On day 5, RAM2061 or ZA was added and after 48 h incubation, cells were removed by adding 5% sodium hypochlorite to each well for 3-5 min. Pit areas were imaged using an EVOS cell imaging microscope at 2x magnification and resorptive area was measured using Image Lab software.

Immunofluorescent microscopy

RAW264.7 cells were differentiated on glass coverslips over the span of 4 days. On day 5, cells were fixed with 4% paraformaldehyde for 15 min, permeabilized in 0.5% Tween-20 for 1 h, and blocked in 5% goat serum for 1 h RT. Cells were then stained 1:300 with Cdc42 primary antibody in 5% goat serum overnight at 4 °C. Following incubation, coverslips were washed in 1x PBS and stained with fluorescent secondary antibody (Alexa Flour 594) for 1 h RT. Similarly, differentiated cells on day 5 were permeabilized and stained 1:300 with Flash Phalloidin Green 488 (Invitrogen) in 1x PBS for 30 min. Coverslips were washed 4 times in PBS, let to dry,

and mounted with DAPI medium. Images were obtained using a Zeiss 710 confocal laser scanning microscope. Table S1 summarizes the antibodies used in these microscopy studies.

Animals

A total of 15 female CD-1 mice (Charles River) between ages of 6 and 8 weeks were housed in the University of Nebraska Medical Center (UNMC) Comparative Medicine facility at a temperature of 23-25 °C, relative humidity of 50%-70%, and 12/12 h light/dark cycles. Mice were socially housed in individually ventilated cages and fed autoclaved Envigo 7012 diet ad libitum. The UNMC Institutional Animal Care and Use Committee approved all studies (protocol no. 16-132-11-FC).

Drug administration

Mice were divided into control and treatment groups ($n = 5$ per group) and treated 2x weekly with PBS (solvent control) administered intravenous (IV) via tail vein, RAM2061 (0.08 mg/kg, IV), or ZA (125 μg/kg) administered subcutaneously for a total of 3 weeks. Mice were euthanized via carbon dioxide asphyxiation 96 h post final dose and necessary tissues were collected. Investigators were not blinded during animal handling nor while conducting downstream experimental readouts.

Blood analysis

Blood samples were obtained post-mortem from the heart and collected in lithium-heparin coated tubes. Following centrifugation, plasma was collected and stored at −80 °C. Commercial ELISA kits (Novus Biologics) were utilized for measuring plasma levels of TRAP5b (NBP2-76463), c-terminal telopeptide (CTX) (NBP2-82400), and procollagen type I N-propeptide (P1NP) (NBP2-76466). Assays were performed according to the manufacturer protocols.

Quantification of RAM2061 accumulation in the bone

Bone marrow was flushed from long bones and bone weight was recorded. All bones were homogenized 1:100 (w/v) based on weight in 15% EDTA solution using a TissueLyserII (Qiagen) and 3 mm tungsten carbide beads (Qiagen). Following homogenization, samples were stored at −20 °C for 2 weeks for decalcification. Bone homogenate (100 μL) was used for quantitation of RAM2061. Samples were diluted in ammonium carbonate buffer (10 mM, 400 μL) with 0.1% NH_4OH in addition to 10 μL of IS RAM1147 (1 μg/mL).[25] The extraction and analysis procedure was followed as previously reported by Chhonker et al.[25] Samples were centrifuged at 5000 g for 5 min, and the supernatant was collected. SPE was conducted using a Strata X-AW, 30 mg extraction cartridge (30 mg/1 mL; Phenomenex, Inc, Torrance, CA). SPE cartridges were preconditioned with 1 mL of methanol followed by 1 mL of ammonium carbonate buffer. Samples were then loaded on the SPE cartridge and washed with 1 mL of ammonium carbonate buffer. SPE cartridges were dried under a stream of nitrogen gas and diazomethane (100 μL) solution was added for 15 min. The analytes were eluted with (2 mL) of methanol and dried under nitrogen in a water bath at 50 °C. Dry residues were reconstituted in 100 μL of 0.1% acetic acid-methanol acetonitrile mixture (65:17.5:17.5) and (5 μL) injected into the LC-MS/MS system using previously reported conditions.[25]

Bone microCT analysis

MicroCT analysis was conducted using a Skyscan 1172 X-ray-computed tomography (Skyscan). Imaging was carried out at a voltage of 55 kV and a currency of 181 μA with a medium camera resolution of 2000 × 1000, an aluminum filter of 0.5 mm and pixel size was set to a dimension of 9 μm. Scanning of the left proximal tibia was completed for each sample followed by reconstruction in NRecon software. Acquired images were properly aligned in Dataviewer (Bruker) and uploaded into CTAn (Bruker). The growth plate in the proximal tibia was identified and regions of interest were manually drawn and calculated covering 1 mm starting 50 μm distal to the growth plate. Trabecular parameters such as bone volume fraction (BV/TV), trabecular thickness (Tb.Th), trabecular separation (Tb.Sp), and trabecular number (Tb.N) were quantified and representative 3D images were constructed in CTAvol (Bruker).

Histology

Mouse bones were fixed in 10% buffered formalin for 24 h at 4 °C, washed in PBS, and decalcified in 15% EDTA for 2 weeks. Bones were embedded and sectioned by the UNMC Tissue Science Facility, then deparaffinized and hydrated through a series of ethanol gradients. For TRAP staining, slides were incubated for 30 min at RT in buffer solution (0.2 M sodium acetate buffer pH 5.2, 50 mM sodium tartrate dihydrate). Following addition of naphtol AS-BI substrate (0.5 mg/mL buffer) and Fast Red Salt TR (1 mg/mL buffer), slides were incubated in staining solution for 1 h at 37 °C protected from light. Slides were washed in ddH_2O and counterstained in hematoxylin for 1 min. Slides were mounted with permount and images were collected using a Zeiss Axioscan 7 whole slide imaging system. To quantify osteoclast numbers, the most distal part of the growth plate was identified and from there a distance of approximately 1000 μm was established in which osteoclast (TRAP+ cells with ≥2 nuclei on the bone surface) numbers were recorded.

Statistical analysis

Two-tailed t-tests were utilized for calculating statistical significance. An α of 0.05 was set as the level of significance. IC_{50} values were determined using Compusyn software version 1.0.1.

Results

RAM2061 depletes intracellular GGPP levels and disrupts protein geranylgeranylation in undifferentiated RAW264.7 cells in a concentration-dependent manner.

To elucidate the effects of GGSI RAM2061 (structure shown in Figure 1A) on osteoclast biology, we first examined whether RAM2061 binds to bone. We conducted HAP binding experiments from which we determined RAM2061 to have 59 ± 5.9% binding affinity compared with >95% binding affinity reported for ZA.[27] Having confirmed that our GGSI has bone affinity we next set out to evaluate on-target activity using the mouse macrophage RAW264.7 cell line, which, when stimulated with osteoclast differentiation factor RANKL, develops into mature multinucleated osteoclasts.[28] Using a previously developed LC-MS/MS methodology,[26] we confirmed that RAM2061 treatment significantly depletes intracellular GGPP levels to below the level of quantitation,

with a trend toward increasing FPP levels following 48 h treatment (Figure 1B). Using ZA as a positive control (Figure 1A), we confirmed depletion of GGPP with a corresponding trend toward decreased FPP, consistent with activity as an FDPS inhibitor. To establish that depletion of GGPP results in impairment in protein geranylgeranylation, immunoblot analysis was performed using an antibody specific for the non-geranylgeranylated form of Rap1a. We determined that RAM2061 disrupts geranylgeranylation in undifferentiated cells in a concentration-dependent manner (Figure 1C), which was also evident following ZA treatment (Figure S1B). MTT cytotoxicity assays revealed a concentration-dependent response following 48 or 72 h treatment (Figure 1D). The 48 h IC_{50} was 307 ± 49 nM and 510 ± 43 nM at 72 h. Therefore, for all additional in vitro studies, we used either 200 or 400 nM, as these concentrations yielded on-target effects without inducing substantial cytotoxicity. Similarly, MTT assays were conducted using ZA to determine appropriate concentrations (Figure S1A).

Disruption of geranylgeranylation induces the UPR pathway and apoptosis in undifferentiated RAW264.7 cells.

To investigate further the consequences of disrupting protein geranylgeranylation, we analyzed changes in expression of UPR-specific genes. Using IBP inhibitors lovastatin and ZA as controls for disruption of geranylgeranylation, qRT-PCR analysis revealed that incubation with RAM2061 for 24 h significantly upregulates transcription of multiple UPR markers, including activating transcription factor 4 (ATF4), inositol-requiring enzyme 1 (IRE1), and protein kinase RNA-like ER kinase (PERK) (Figure 2A). Similarly, 48 h incubation was associated with increased expression of ATF6 and IRE1, as well as C/EBP homologous protein (CHOP), which is responsible for the apoptotic arm of the UPR pathway. Analysis of x-box binding protein 1 (XBP1) splicing, which is a downstream process in the IRE1 arm of the UPR, revealed evidence of splicing at both 24 and 48 h time points in RAM2061-treated cells (Figure 2B). UPR pathway activation was further confirmed with immunoblot analysis, which demonstrated upregulation of ATF4 and phosphorylation of eukaryotic translation initiation factor 2α (eIF2α), with a robust activation at the 48 h timepoint (Figure 2C). To confirm whether UPR induction leads to apoptosis, we examined poly-ADP-ribose polymerase (PARP) and caspase cleavage. Cleavage of PARP and caspases-3, -8, and -9 was observed at 48 h (Figure 2C). We next conducted a GGPP co-incubation experiment to confirm that the effects of RAM2061 on the UPR and apoptosis are a consequence of depletion of intracellular GGPP. As shown in Figure 2D, co-incubation of RAM2061 with GGPP restored protein geranylgeranylation, abrogating induction of UPR activation and apoptosis. In conclusion, we found RAM2061 to demonstrate on-target activity in undifferentiated RAW264.7 cells by depleting intracellular GGPP, disrupting protein geranylgeranylation, activating the UPR, and inducing apoptosis.

GGSI treatment disrupts osteoclast differentiation leading to decreased osteoclast numbers and abnormal osteoclast morphology.

We next focused on understanding the effects of GGDPS inhibition on osteoclast differentiation and function. Treatment of RAW264.7 cells with osteoclast differentiation factor RANKL is known to induce mature osteoclast formation.[29,30] While differentiation of RAW264.7 cells in vitro does not require the addition of exogenous M-CSF, we determined that the addition of M-CSF on the day of plating increased osteoclast yield. Therefore, cells were seeded in the presence of recombinant M-CSF followed by the daily addition of recombinant RANKL for 4 days. We treated cells with RAM2061 or ZA on day 1 (D1) and on day 5 (D5) cells were fixed and stained for TRAP activity. TRAP is an enzyme secreted by osteoclasts during bone resorption, and TRAP expression is a widely used marker for osteoclast lineage and activity.[31] The addition of RAM2061 on D1 of differentiation significantly decreased TRAP-positive osteoclast formation, with resulting osteoclasts being smaller and lacking a continuous, round outer ring (Figure 3A and B). Analysis of secreted TRAP activity in the cell culture media indicated decreased activity following GGSI treatment (Figure 3C), suggesting potential for diminished osteoclast resorptive ability comparable with ZA. We evaluated effects on osteoclast-specific marker expression via qRT-PCR. While demonstrating no statistically significant effects on gene expression at the 200 nM concentration, 400 nM RAM2061 treatment significantly decreased expression of not only TRAP *(ACP5)* but also osteoclast-specific protease cathepsin K *(CTSK)* and osteoclast-master transcription factor nuclear factor of activated T-cells 1 *(NFATc1)* (Figure 3D).

We also investigated whether adding RAM2061 on day 3 (D3) during differentiation impacted osteoclast numbers and activity. Similar to osteoclasts treated on D1, we observed statistically significant decreases in TRAP-positive osteoclast numbers and TRAP activity in the media, although to a lesser extent than what was seen with D1 treatment (Figure S2A,B, and C). D3-treated osteoclasts receiving 400 nM RAM2061 also demonstrated decreased expression of *ACP5, CTSK,* and *NFATc1* (Figure S2D).

RAM2061 demonstrates on-target activity in fully differentiated osteoclasts and anti-resorptive effects.

Next, we were interested in determining the effects of GGSI treatment on fully differentiated osteoclasts. Following the 5-day differentiation period, osteoclasts were incubated with varying concentrations of RAM2061 and MTT cytotoxicity assays and immunoblot analyses were performed. RAM2061 exerts concentration-dependent effects with a more robust response at 48 and 72 h compared with 24 h (Figure 4A). We confirmed on-target activity of RAM2061 in mature osteoclasts with evidence of disruption of protein geranylgeranylation at 48 h following either sub-IC_{50} concentrations 200 or 400 nM treatment (Figure 4B). Additional MTT assays were conducted to confirm ZA activity in mature osteoclast cells (Figure S1A).

We then determined the impact of RAM2061 treatment on osteoclast activity. Following osteoclast differentiation, cells were treated with RAM2061 or ZA for 48 h. On day 7 (D7) cells were fixed and stained with TRAP. We found that RAM2061 treatment reduced TRAP-positive osteoclast numbers in a concentration-dependent manner (Figure 4C,D). Similarly, levels of secreted TRAP were significantly reduced following RAM2061 treatment (Figure 4E). To confirm corresponding anti-resorptive effects, we utilized commercially available HAP-coated plates on which RAW264.7 cells were differentiated and then treated with RAM2061 or ZA for 48 h. Following drug treatment, cells were removed from the plate and pit formation was quantified using Image Lab software (Figure 4F). We found that RAM2061 disrupts osteoclast resorption in a concentration-dependent manner

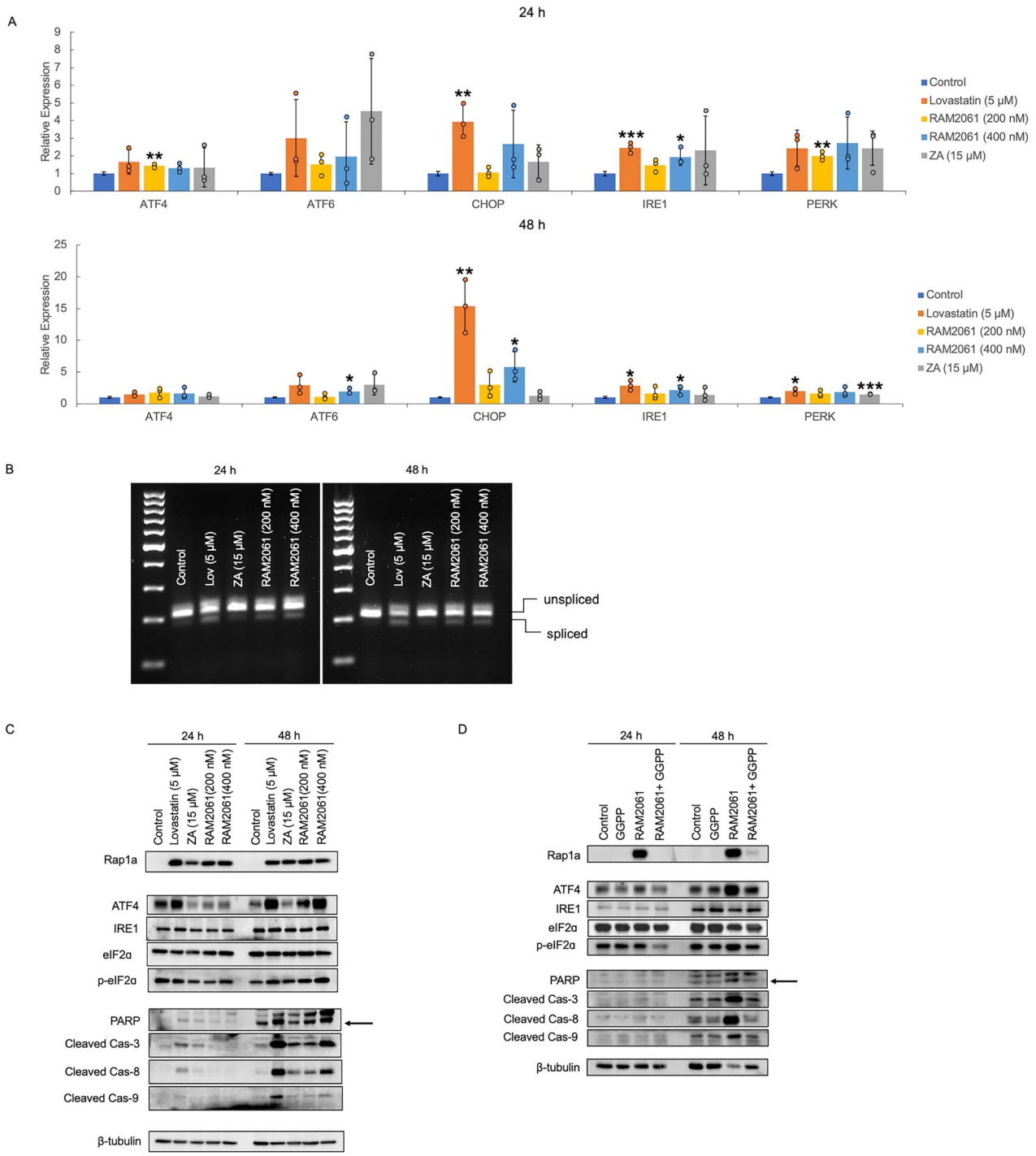

Figure 2. Geranylgeranyl diphosphate synthase (GGDPS) inhibitor (GGSI) treatment of undifferentiated RAW264.7 cells induces unfolded protein response (UPR) activation and apoptosis. (A) Quantitative real-time polymerase chain reaction analysis of UPR markers ATF4, ATF6, CHOP, IRE1, and PERK following incubation of RAW264.7 cells in the presence or absence of lovastatin (5 μM), zoledronic acid (ZA) (15 μM), or RAM2061 (200 or 400 nM) for 24 or 48 h. Data represent fold-change normalized to control ($n = 3$ biological replicates, data are represented as mean ± SD; * denotes $p < .05$, ** denotes $p < .01$, *** denotes $p < .001$). (B) Analysis of XBP1 splicing following incubation of RAW264.7 cells in the presence or absence of lovastatin (5 μM), ZA (15 μM), or RAM2061 (200 or 400 nM) for 24 or 48 h. Images are representative of 3 independent experiments. (C) RAW264.7 cells were incubated in the presence or absence of lovastatin, ZA, or RAM2061 for 24 or 48 h. Immunoblot analysis for unmodified Rap1a (Rap1a), UPR markers (ATF4, IRE1, p-e1F2α, e1F2α), apoptotic markers (PARP [arrow = cleaved PARP], cleaved caspases 3, 8, and 9) and β-tubulin (loading control) was performed. Immunoblots are representative of 3 independent experiments. (D) RAW264.7 cells were incubated in the presence or absence of RAM2061 (400 nM) and/or exogenous geranylgeranyl diphosphate (GGPP, 10 μM) for 48 h. Immunoblot analysis for unmodified Rap1a (Rap1a), UPR markers (ATF4, IRE1, p-e1F2α, e1F2α), and apoptotic markers (PARP (arrow = cleaved PARP), cleaved caspases 3, 8, and 9). β-tubulin is shown as the loading control. Immunoblots are representative of 3 independent experiments.

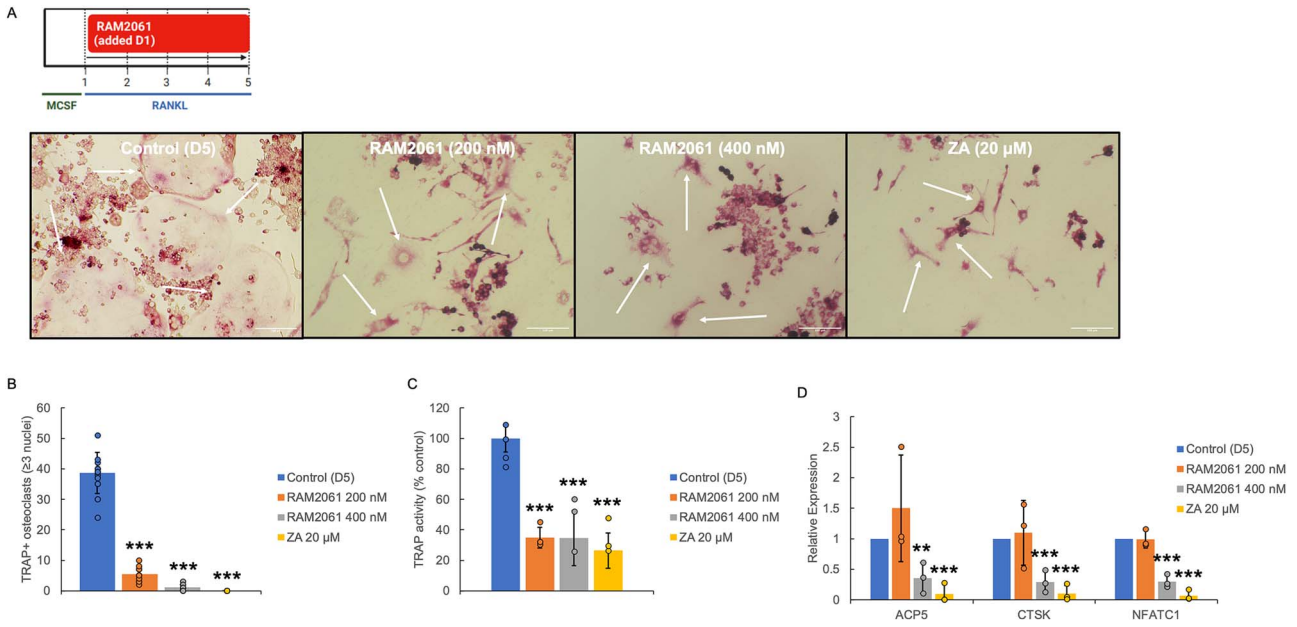

Figure 3. GGSI treatment disrupts osteoclast differentiation. RAW264.7 cells were differentiated over a span of 5 days in the presence or absence of RAM2061 (200 or 400 nM) or ZA (20 μM) (added on day 1 (D1)) (schema in A). On day 5 (D5), cells were fixed and stained with tartrate resistant acid phosphatase (TRAP) to evaluate TRAP-positive osteoclast formation. (A) Images were taken on an EVOS cell imaging microscope at 20x magnification (images are representative of 3 independent experiments; scale bar = 100 μm; arrows indicate multi-nucleated osteoclasts). (B) Total osteoclast number per well was quantified based on TRAP+ staining and the presence of 3 or more nuclei ($n = 3$ biological replicates, data are represented as mean ± SD, *** denotes $p < .001$ per t-test). (C) On day 5, media was collected in order to measure levels of secreted TRAP activity ($n = 3$ biological replicates; data represent secreted TRAP enzymatic activity as percent control ± SD, *** denotes $p < .001$ per t-test). (D) Quantitative real-time polymerase chain reaction analysis of osteoclast markers ACP5, CTSK, and NFATc1 following incubation in the presence or absence of RAM2061 (200 or 400 nM) or ZA (20 μM) added on day 1 during the differentiation period. On day 5, RNA was extracted and expression was quantified as fold change normalized to control ($n = 3$ biological replicates, data are represented as mean ± SD; ** denotes $p < .01$, *** denotes $p < .001$ per t-test).

and that the effects were comparable with ZA, but at nearly 50-100-fold lower concentration compared with ZA. Therefore, we determined that RAM2061 demonstrates anti-osteoclastic effects, disrupting both cell differentiation and resorptive function.

RAM2061 disrupts Rho GTPase localization, inhibiting proper actin ring formation.

The anti-osteoclastic effects of NBPs are attributed to disruption of Rho cytoskeletal processes, ultimately disrupting F-actin ring formation and osteoclast resorption.[7,13] Therefore, we investigated whether GGSI treatment induced similar effects. Utilizing immunofluorescent microscopy, we differentiated RAW264.7 cells on glass coverslips for the standard 5-day period. Cells were differentiated in the presence or absence of RAM2061 or ZA and on D5 cells were fixed and stained for identification of the Rho GTPase Cdc42. In control (untreated) osteoclasts, Cdc42 is seen localizing to the edges of the basolateral membrane where the actin ring has formed (Figure 5A). Following treatment with RAM2061, localization of Cdc42 to the outer membrane is lost with resulting accumulation in the cytosol. The effects on actin ring morphology were evaluated with phalloidin staining. The RAM2061-treated osteoclasts lacked cohesive outer actin ring formation and were much smaller in size with around 2-3 nuclei compared with control with ≥10 nuclei (Figure 5B). ZA-treated osteoclasts demonstrated a similar phenotype being much smaller in size with around 3-4 nuclei. This suggests that GGSI inhibition of Rho protein geranylgeranylation leads to mislocalization of the proteins with subsequent loss of actin regulatory function.

When examining the effects of GGSI treatment on fully differentiated osteoclasts, 48 h RAM2061 treatment also resulted in mislocalization of Cdc42 to the cytosol with osteoclasts being much smaller in size (Figure 5C). However, the effects on actin ring formation were less pronounced (Figure 5D) relative to the effects observed when drug was present throughout the differentiation period (Figure 5B). Of note, we also investigated the effects of adding drug in the middle of the differentiation period. RAM2061 treatment led to Cdc42 mislocalization and inconsistent outer ring formation when the drug was added on D3 (Figure S3). These osteoclasts usually had around 3-4 nuclei, suggesting that duration of treatment throughout the differentiation process may have different impacts on actin ring formation and morphology.

Assessing the impact of GGSI treatment on normal bone remodeling in vivo.

To elucidate whether the observed anti-resorptive effects are recapitulated in vivo, we injected 6-8 week old female CD-1 mice with either PBS (vehicle), RAM2061 (0.08 mg/kg IV), or ZA (125 μg/kg SC) 2x weekly for 3 weeks (Figure 6A). No adverse events were noted during the treatment period. Mice were sacrificed 96 h post-final dose at which point plasma, tibias, femurs, and mandibles were collected. Plasma was used for the analysis of bone turnover makers including TRAP5b and CTX (indicative of bone resorption) and P1NP (indicative of bone formation). We did not observe any significant changes in plasma concentrations of bone turnover markers across all treatment groups (Figure S4A). Following homogenization and decalcification of the bone samples, immunoblot

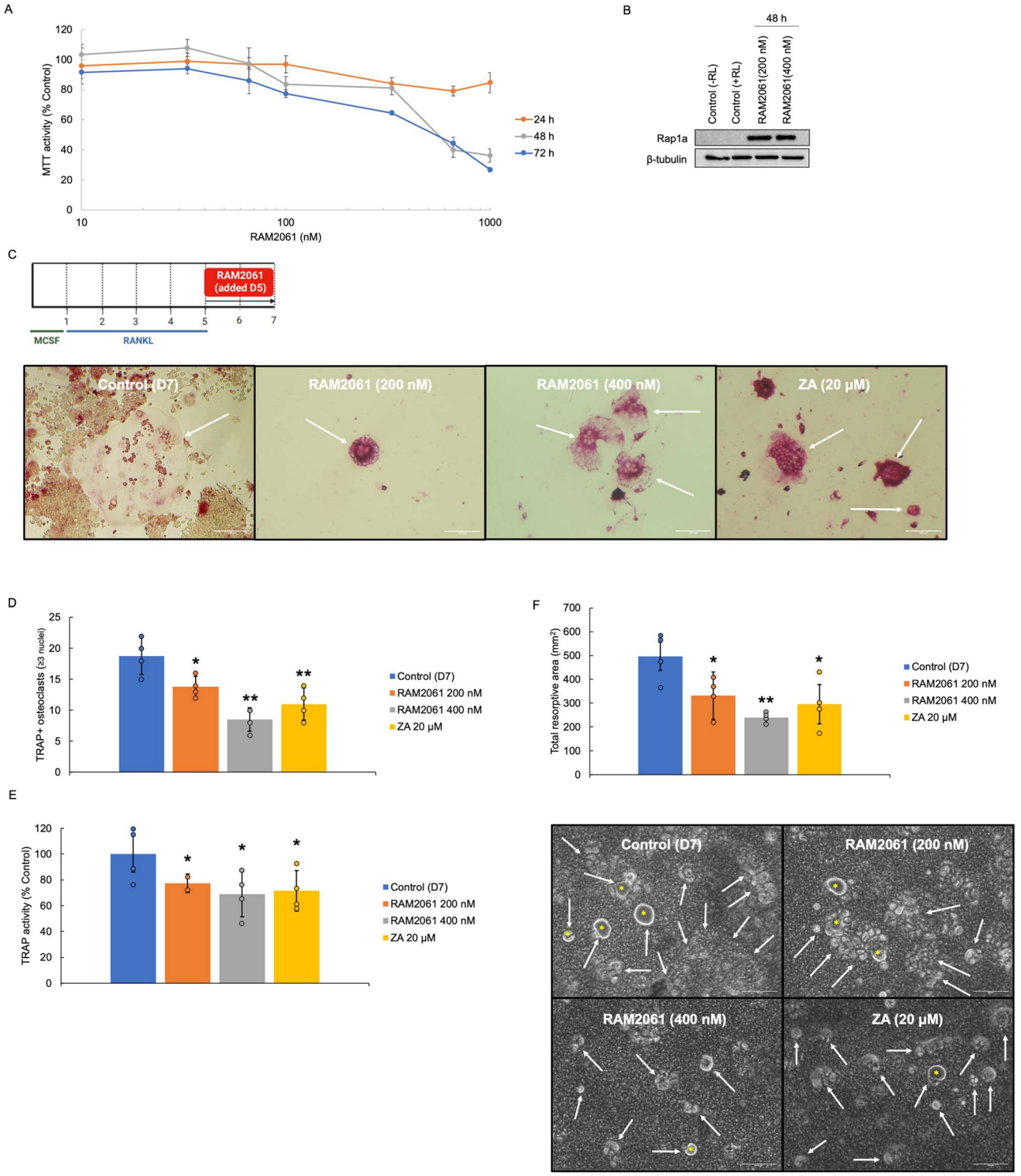

Figure 4. GGSI treatment of mature osteoclasts disrupts protein geranylgeranylation and decreases osteoclast number and resorptive function. RAW264.7 cells were differentiated over a span of 5 days and then either RAM2061 or zoledronic acid (ZA) was added on day 5. (A) MTT assays were performed following a 24, 48, or 72 h incubation with RAM2061 ($n = 4$, data are displayed as mean ± SD). (B) Immunoblot analysis for unmodified Rap1a (Rap1a) and β-tubulin (loading control). -RL = RAW264.7 not stimulated with receptor activator of nuclear factor-κB ligand (RANKL); +RL = RAW264.7 differentiated with RANKL. Immunoblots are representative of 3 independent experiments. (C) Schema of differentiation showing timing of RANKL and macrophage colony stimulating factor (MCSF) treatment as well as drug treatment. Following the addition of RAM2061 (200 or 400 nM) or ZA (20 μM) on day 5, cells were fixed on day 7 (D7) and stained with tartrate resistant acid phosphatase (TRAP) to evaluate TRAP-positive osteoclast formation. Images were taken on an EVOS cell imaging microscope at 20x magnification (images are representative of 3 independent experiments; scale bar = 100 μm). (D) Total osteoclast number per well was quantified based on TRAP+ staining and the presence of 3 or more nuclei ($n = 3$ biological replicates, data are represented as mean ± SD, * denotes $p < .05$, ** denotes $p < .01$ per t-test). (E) On day 7, media was collected, and secreted TRAP activity was measured and normalized to control ($n = 3$ biological replicates; data are displayed as mean ± SD, * denotes $p < .05$ per t-test). (F) RAW264.7 cells were differentiated over the span of 5 days on hydroxyapatite-coated plates with the subsequent addition of RAM2061 (200 or 400 nM) or ZA (20 μM) on day 5. On day 7, cells were removed and the resorptive area was quantified using ImageLab. Representative images of the resorptive areas taken on an EVOS cell imaging microscope at 20x magnification) ($n = 4$ biological replicates, data represented as mean ± SD, * denotes $p < .05$, ** denotes p < .01 per t-test). The arrows indicate resorbed areas; * indicate pits where the entire hydroxyapatite coating was resorbed.

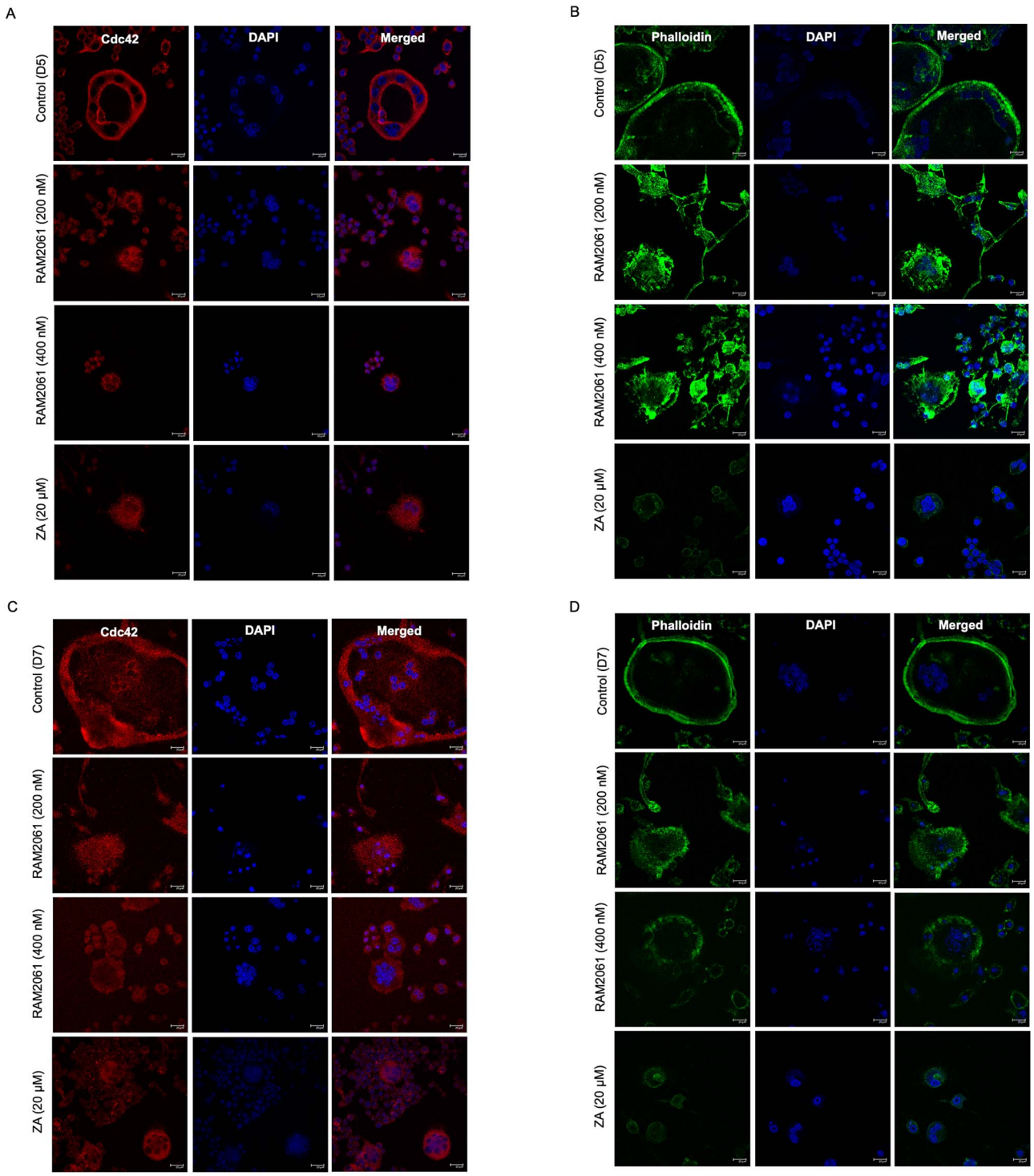

Figure 5. GGSI treatment disrupts Cdc42 GTPase localization and subsequent regulation of actin dynamics necessary for osteoclast differentiation and actin ring formation. RAW264.7 cells were differentiated on glass coverslips over a span of 5 days and RAM2061 (200 or 400 nM) or zoledronic acid (ZA) (20 μM) was added on day 1. (A) On day 5 (D5), osteoclasts were fixed and stained with an antibody against Cdc42 and DAPI (nucleus label) or (B) stained with phalloidin for identification of actin and DAPI (nuclei). (C) Fully differentiated D5 osteoclasts were treated with RAM2061 (200 or 400 nM) or ZA (20 μM) for 48 h. On day 7 (D7), osteoclasts were fixed and stained with an antibody against Cdc42 and DAPI (nucleus label) or (D) stained with phalloidin (actin) and DAPI (nuclei). Images were obtained using a Zeiss 710 LSM at 40x magnification. Images are representative of 3 independent experiments (scale bar = 20 μm).

analysis was performed to confirm disruption of geranylgeranylation, as evidenced by the presence of unmodified Rap1a (Figure 6B). We confirmed accumulation of RAM2061 in the bone samples by utilizing LC-MS/MS quantification (Figure 6C).

To characterize the effects of RAM2061 on bone density and morphometry, we conducted microCT analysis of the left proximal tibia specimens. ZA significantly increased trabecular bone volume (BV/TV) (p=.02) and trabecular number (Tb.N; p=.004) compared with control, while RAM2061

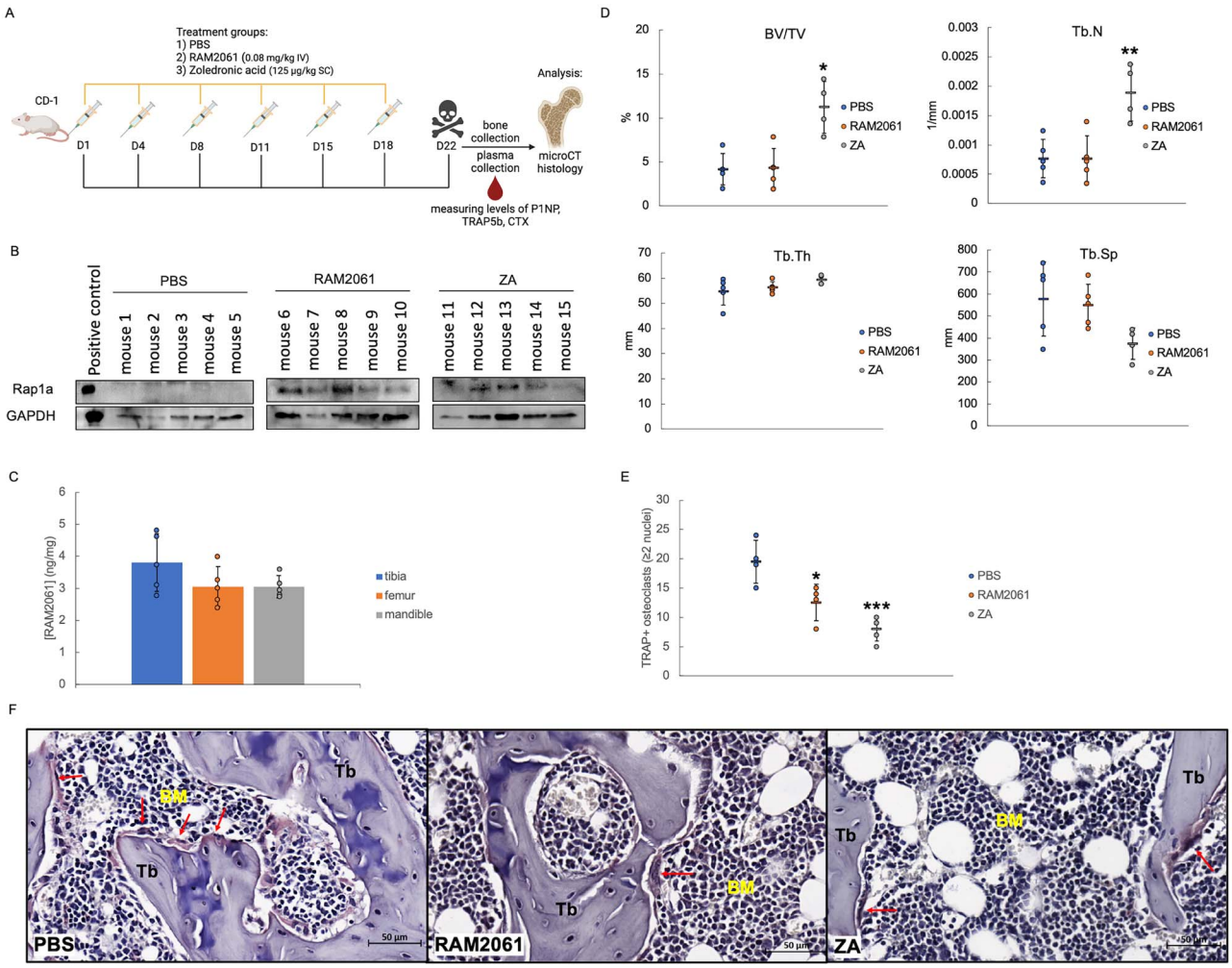

Figure 6. RAM2061 does not significantly impact normal bone remodeling in CD-1 mice. (A) Schematic representation of drug administration/dosing and downstream readouts conducted. Abbreviations: procollagen type 1 N-propeptide (P1NP); C-terminal telopeptide (CTX), tartrate resistant acid phosphatase 5b (TRAP5b). (B) Immunoblot analysis of unmodified Rap1a and GAPDH (loading control) using 30 μL of bone homogenate from long bones of mice; positive control = cell lysate from RAW264.7 osteoclasts (D5) treated with 400 nM RAM2061 for 48 h). (C) Quantification of RAM2061 accumulation in long bones and mandibles of CD-1 mice ($n = 5$ per group, data are represented as mean ± SD). (D) MicroCT analysis portraying morphometric analysis of the proximal tibia specimens. Individual data points are shown with mean ± SD (PBS $n = 5$; RAM2061 $n = 5$; zoledronic acid (ZA) $n = 4$; * denotes $p < .05$, ** denotes $p < .01$ per t-test). (E) The growth plate in the distal femur of tartrate resistant acid phosphatase (TRAP)-stained sections were identified and 1000 μm from the most distal area was used to encapsulate the area of interest. Quantification of osteoclast numbers in the defined area per femur was performed. Individual data points are shown with mean ± SD (PBS $n = 5$; RAM2061 $n = 4$; ZA $n = 4$, * denotes $p < .05$, *** denotes $p < .001$ per t-test). (F) Representative images of TRAP-stained sections of distal femurs (scale bar = 50 μm). The arrows indicate TRAP+ osteoclasts (Tb = trabecular bone, BM = bone marrow).

demonstrated no statistically significant changes in these parameters (Figure 6D). Statistically significant changes in other measures of trabecular bone structure such as trabecular thickness (Tb.Th) and trabecular separation (Tb.Sp) were not observed in either treatment group. Representative cross sections and 3D models of each treatment visually recapitulate the increase in bone volume demonstrated by the ZA group (Figure S4B and C). We also conducted TRAP staining of the femur specimens (Figure 6E and F). Quantification of osteoclast numbers in the distal femur revealed a significant decrease in TRAP-positive numbers in both RAM2061- and ZA-treated mice (Figure 6E).

Discussion

These studies are the first to report the effects of GGSI treatment on osteoclast function and bone remodeling. Our in vitro studies revealed that GGSI treatment induces anti-osteoclastic effects comparable with the frontline bone-strengthening agent ZA. These studies support an underlying mechanism involving disruption of Rho protein geranylgeranylation preventing regulation of actin dynamics necessary for osteoclast differentiation and function. We also demonstrate for the first time that the GGSI RAM2061 has affinity for HAP and accumulates in the bone following administration in vivo. Following a 3-week treatment period in young CD-1 mice, RAM2061, unlike ZA, did not significantly impact morphological parameters of bone remodeling. However, TRAP staining of distal femora revealed RAM2061 does significantly decrease TRAP+ osteoclast numbers, warranting investigation of its effects in osteolytic diseases such as MBD.

Osteoclast cells are a highly specialized cell type that rely heavily on Rho GTPases for proper differentiation and function. Various knockout and loss of function experiments have found GTPases Cdc42 and Rac1 to be essential for osteoclast

viability and function, with Rac1 primarily recognized for its role in early cell-cell fusion events necessary for osteoclast multinucleation, and Cdc42 primarily regulating osteoclast polarization and sealing zone formation.[32–35] It is noted that the undifferentiated RAW264.7 cells were more sensitive to the cytotoxic effects of RAM2061 compared with the differentiated cells, similar to what was observed with ZA. While the observed effects of RAM2061 (or ZA) on osteoclast differentiation and function may in part be due to decreased numbers of osteoclast precursors and/or osteoclasts secondary to apoptosis, it is also evident that GGSI treatment led to direct effects on osteoclasts secondary to impaired GTPase function. Our microscopy studies demonstrated that GGSI treatment resulted in mislocalization of Cdc42 and disruption of actin ring formation. It is also noted that Rab GTPases play roles in osteoclast intracellular trafficking necessary for acidification of the sealing zone and for release of resorbed proteins.[36–38] While we did not specifically evaluate the effect of RAM2061 on localization of specific Rab proteins, we predict that these processes would also be impaired following GGSI treatment, given the global disruption of geranylgeranylation induced by inhibition of GGDPS.

It is important to recognize that osteoclast cytoskeletal dynamics vary based on the substrate they are cultured on, with the interaction of bone itself initiating the resorption process. Therefore, the osteoclasts evaluated in the confocal microscopy studies were not undergoing active resorption.[39] Our studies evaluating GGSI treatment effect on osteoclasts grown on HAP-coated plates more directly addressed the impact on resorptive activity, particularly the impact on the acidification process that occurs during bone resorption.

While we did not specifically focus on the effects of GGSI treatment on osteoblast differentiation and function, previous studies have found NBPs to provide a pro-osteoblastic effect attributed to depletion of GGPP.[5,40–44] However, studies involving the GGSI digeranyl bisphosphonate (DGBP) in MC3T3-E1 cells have suggested that resulting FPP accumulation leads to glucocorticoid receptor activation, ultimately inhibiting osteoblast differentiation and mineralization.[42] It is important to note that RAM2061 is a significantly more potent GGSI than DGBP in cell culture experiments (eg, in myeloma cells, $\geq$25 nM of RAM2061 vs $\geq$10 μM of DGBP is required to exert effects)[20,24,45] and that only in vitro experiments were conducted with DGBP,[42] suggesting need for further investigation into the effects of RAM2061 on osteoblast biology in vivo.

Previous work done in 6-week old BALB/c mice demonstrated that a single clinically relevant dose of ZA could significantly increase trabecular bone volume in as early as 3 days post-administration, with such effects maintained for at least 10 days.[46] As our previous preclinical studies established dosing in 6-8 week old outbred CD-1 mice, we used this animal model as a preliminary assessment of the impact of GGSI treatment on bone remodeling. Interestingly, while this model did confirm the anti-resorptive properties of ZA, we found GGSI treatment to have no statistically significant effects on bone resorption or bone formation parameters, although a decrease in osteoclast number was observed (Figure 6). Since our in vitro experiments revealed RAM2061 to have anti-osteoclastic effects comparable with ZA at nearly 50-100-fold lower concentrations, we hypothesize that such differences in vivo are due to variation in bone affinity, pharmacokinetics, and biodistribution parameters. To evaluate RAM2061's bone affinity we conduced HAP binding experiments and determined that RAM2061 exhibits 60% HAP affinity compared with the >95% reported for ZA.[47] Extensive structure-function studies have revealed the importance of chemical makeup on bone affinity and extent of antiresorptive effects. While the P-C-P backbone of BPs is essential for binding to the calcium HAP of the bone, other structural factors such as the presence of an α-hydroxy group on the geminal carbon, the number and position of nitrogen atoms, and the addition of alkyl substituents or methylene groups all impact NBP bone affinity and binding.[47–49] For example, the relationship between structure and bone affinity has previously been assessed by manipulating the structure of the NBP risedronate in which loss of the α-hydroxy group was found to decrease HAP binding by approximately 60%.[48,50] RAM2061 is also an NBP, with the nitrogen-containing ring being a triazole, while having a methyl group at the α-position and a homoneryl tail (Figure 1A). These structural differences not only likely account for the reduced HAP affinity relative to ZA, but also contribute to its unique pharmacokinetic and biodistribution properties.[15] Our histology studies from the in vivo experiment revealed a decrease in osteoclast number similar to ZA, suggesting the observed differences in effects on bone remodeling parameters may be due to factors such as binding to the bone matrix, rates of drug turnover in the bone, and impact on other types of bone cells.

ZA is eliminated by a triphasic process with an initial rapid biphasic clearance, with 40% of the total dose recovered in the urine 24 h post-infusion, followed by a long terminal elimination phase with a half-life of up to half a year.[12] During this terminal elimination phase, ZA undergoes a cycling between plasma and the bone as bone remodeling takes place. This is a slow process with only 60% of ZA cleared after 12 months suggesting long-term retention in bone.[12] In contrast, we have found RAM2061 to have a prolonged plasma half-life of 29.2 ± 6 h with systemic distribution to various tissues.[15] We did confirm accumulation of RAM2061 in bone following the 3-week treatment course (Figure 6C), but future studies will be needed to determine whether there is a prolonged terminal elimination phase. Overall, these factors likely account for the disparate results observed following short-term treatment with RAM2061 vs ZA.

While we did not observe significant anti-resorptive effects from RAM2061 treatment in the process of normal bone remodeling in young mice, the effects may be different with more prolonged treatment and/or in the setting of bone disease. A limitation to our in vivo model could be due to the age of the mice. Unlike humans, bones of mice continue to grow after sexual maturity, therefore these 6-8 week old mice were still undergoing significant bone remodeling.[51] This could explain the observed variation in the bone turnover markers and architecture of the control mice, possibly impacting the bone turnover changes in mice treated with RAM2061.

Bone-related diseases such as MBD and some bone metastatic cancers are known to result from disruption of the normal bone remodeling cycle. In the case of osteolytic diseases specifically, such disruption leads to diminished bone mineral density increasing risk of pathological fracture. Since we have previously found RAM2061 to have anti-neoplastic effects, specifically in the case of multiple myeloma, it will be important to determine whether GGSI treatment is able to restore balance in the remodeling cycle through apoptosis of

the malignant cells responsible for disrupting the normal bone microenvironment. These effects would be unique compared with NBPs, which, while demonstrating anti-neoplastic effects in vitro, lack sufficient anti-cancer activity in vivo as a result of appreciable systemic distribution.[8–10,12,52] Efforts to achieve distribution to tumor have focused primarily on formulation of NBP nanoparticles, but drug loading capacity and premature release problems have been challenges.[53,54] In addition, the drawback of ZA's very high bone affinity and prolonged bone exposure is the development of osteonecrosis of the jaw. Thus, there are potential advantages to the development of agents, which are characterized by both moderate bone affinity and direct anti-osteoclastic activity in addition to having sufficient systemic distribution to yield direct anti-neoplastic activity.

In conclusion, these studies have demonstrated that GGSI treatment exerts anti-osteoclastic effects in vitro, suggesting potential for anti-resorptive effects in vivo. Future studies will focus on further defining the pharmacokinetic properties of RAM2061 with respect to the bone compartment, including initial uptake, release, and redistribution parameters. Furthermore, evaluation of GGSI treatment in models of MBD and osteolytic bone metastatic cancers will be required to delineate both the direct (due to effects on osteoclasts) and indirect (due to anti-neoplastic effects) impact on bone disease.

Acknowledgments

We acknowledge the use of the University of Nebraska Medical Center (UNMC) Advanced Microscopy Core Facility, RRID:SCR_022467, P20GM103427 (NIGMS, NE-INBRE), P30GM106397 (NIGMS, NCCS), P20GM130447 (NIGMS, CoNDA), P30CA036727 (NCI, Buffett Cancer Center), S10RR027301(NIH), S10OD030486 (NIH), Nebraska Research Initiative, UNMC Vice Chancellor for Research Office. We also acknowledge the use of the UNMC Tissue Sciences Facility. We would also like to acknowledge Xiaoqing Du of the Dong Wang lab (UNMC) for conducting the microCT scans and reconstruction.

Author contributions

Molly Muehlebach (Conceptualization, Data curation, Formal analysis, Investigation, Methodology, Writing—original draft, Writing—review & editing), Staci Haney (Investigation, Supervision, Writing—review & editing), Yashpal Chhonker (Investigation, Supervision), Mamunur Rashid (Formal analysis, Investigation, Methodology, Writing—review & editing), Daryl Murry (Formal analysis, Methodology, Supervision, Writing—review & editing), Geoffrey Talmon (Formal analysis, Writing—review & editing), and Sarah Holstein (Conceptualization, Formal analysis, Funding acquisition, Project administration, Supervision, Writing—review & editing)

Supplementary material

Supplementary material is available at *JBMR Plus* online.

Funding

This work was supported by the National Institutes of Health (Grants P30 CA036727 and R01 CA258621) and funding from the University of Nebraska Medical Center Graduate Studies Assistantship (awarded to MEM).

Conflicts of interest

The authors have no conflicts of interest.

Data availability

The data underlying this article are available in the article and in its online supplementary material.

References

1. Roberts PJ, Mitin N, Keller PJ, et al. Rho family GTPase modification and dependence on CAAX motif-signaled posttranslational modification. *J Biol Chem*. 2008;283(37):25150-25163. https://doi.org/10.1074/jbc.M800882200
2. Gomes AQ, Ali BR, Ramalho JS, et al. Membrane targeting of Rab GTPases is influenced by the prenylation motif. *Mol Biol Cell*. 2003;14(5):1882-1899. https://doi.org/10.1091/mbc.e02-10-0639
3. Palsuledesai CC, Distefano MD. Protein prenylation: enzymes, therapeutics, and biotechnology applications. *ACS Chem Biol*. 2015;10(1):51-62. https://doi.org/10.1021/cb500791f
4. Yu Z, Surface LE, Park CY, et al. Identification of a transporter complex responsible for the cytosolic entry of nitrogen-containing bisphosphonates. *eLife*. 2018;7:e36620. https://doi.org/10.7554/eLife.36620
5. van Beek E, Pieterman E, Cohen L, Löwik C, Papapoulos S. Farnesyl pyrophosphate synthase is the molecular target of nitrogen-containing bisphosphonates. *Biochem Biophys Res Commun*. 1999;264(1):108-111. https://doi.org/10.1006/bbrc.1999.1499
6. Coxon FP, Helfrich MH, Van't Hof R, et al. Protein geranylgeranylation is required for osteoclast formation, function, and survival: inhibition by bisphosphonates and GGTI-298. *J Bone Miner Res*. 2000;15(8):1467-1476. https://doi.org/10.1359/jbmr.2000.15.8.1467
7. Holstein SA. A patent review of bisphosphonates in treating bone disease. *Expert Opin Ther Pat*. 2019;29(5):315-325. https://doi.org/10.1080/13543776.2019.1608180
8. Rogers MJ, Mönkkönen J, Munoz MA. Molecular mechanisms of action of bisphosphonates and new insights into their effects outside the skeleton. *Bone*. 2020;139:115493. https://doi.org/10.1016/j.bone.2020.115493
9. Lyseng-Williamson KA. Zoledronic acid: a review of its use in breast cancer. *Drugs*. 2008;68(18):2661-2682. https://doi.org/10.2165/0003495-200868180-00010
10. Jiang P, Zhang P, Mukthavaram R, et al. Anti-cancer effects of nitrogen-containing bisphosphonates on human cancer cells. *Oncotarget*. 2016;7(36):57932-57942. https://doi.org/10.18632/oncotarget.10773
11. Brown J, Paggiosi MA, Rathbone E, et al. Prolonged bone health benefits for breast cancer patients following adjuvant bisphosphonate therapy: the BoHFAB study. *J Bone Miner Res*. 2024;39(1):8-16. https://doi.org/10.1093/jbmr/zjad006
12. Chen T, Berenson J, Vescio R, et al. Pharmacokinetics and pharmacodynamics of zoledronic acid in cancer patients with bone metastases. *J Clin Pharmacol*. 2002;42(11):1228-1236. https://doi.org/10.1177/009127002762491316
13. Fisher JE, Rogers MJ, Halasy JM, et al. Alendronate mechanism of action: geranylgeraniol, an intermediate in the mevalonate pathway, prevents inhibition of osteoclast formation, bone resorption, and kinase activation in vitro. *Proc Natl Acad Sci USA*. 1999;96(1):133-138. https://doi.org/10.1073/pnas.96.1.133
14. Rogers MJ, Gordon S, Benford HL, et al. Cellular and molecular mechanisms of action of bisphosphonates. *Cancer*. 2000;88(12 Suppl):2961-2978. https://doi.org/10.1002/1097-0142(20000615)88:12+<2961::aid-cncr12>3.3.co;2-c
15. Haney SL, Chhonker YS, Varney ML, et al. In vivo evaluation of isoprenoid triazole bisphosphonate inhibitors of geranylgeranyl diphosphate synthase: impact of olefin stereochemistry on toxicity and biodistribution. *J Pharmacol Exp Ther*. 2019;371(2):327-338. https://doi.org/10.1124/jpet.119.258624
16. Haney SL, Varney ML, Chhonker YS, et al. Inhibition of geranylgeranyl diphosphate synthase is a novel therapeutic strategy for

pancreatic ductal adenocarcinoma. *Oncogene*. 2019;38(26):5308-5320. https://doi.org/10.1038/s41388-019-0794-6
17. Haney SL, Feng D, Chhonker YS, et al. Evaluation of geranylgeranyl diphosphate synthase inhibition as a novel strategy for the treatment of osteosarcoma and Ewing sarcoma. *Drug Dev Res*. 2023;84(1):62-74. https://doi.org/10.1002/ddr.22012
18. Zhou X, Ferree SD, Wills VS, et al. Geranyl and neryl triazole bisphosphonates as inhibitors of geranylgeranyl diphosphate synthase. *Bioorg Med Chem*. 2014;22(9):2791-2798. https://doi.org/10.1016/j.bmc.2014.03.014
19. Wills VS, Allen C, Holstein SA, Wiemer DF. Potent triazole bisphosphonate inhibitor of geranylgeranyl diphosphate synthase. *ACS Med Chem Lett*. 2015;6(12):1195-1198. https://doi.org/10.1021/acsmedchemlett.5b00334
20. Matthiesen RA, Varney ML, Xu PC, Rier AS, Wiemer DF, Holstein SA. α-Methylation enhances the potency of isoprenoid triazole bisphosphonates as geranylgeranyl diphosphate synthase inhibitors. *Bioorg Med Chem*. 2018;26(2):376-385. https://doi.org/10.1016/j.bmc.2017.10.023
21. Haney SL, Varney ML, Chhonker Y, et al. In vivo evaluation of combination therapy targeting the isoprenoid biosynthetic pathway. *Pharmacol Res*. 2021;167:105528. https://doi.org/10.1016/j.phrs.2021.105528
22. Haney SL, Varney ML, Williams JT, Smith LM, Talmon G, Holstein SA. Geranylgeranyl diphosphate synthase inhibitor and proteasome inhibitor combination therapy in multiple myeloma. *Exp Hematol Oncol*. 2022;11(1):5. https://doi.org/10.1186/s40164-022-00261-6
23. Haney SL, Chhonker YS, Varney ML, Talmon G, Murry DJ, Holstein SA. Preclinical investigation of a potent geranylgeranyl diphosphate synthase inhibitor. *Investig New Drugs*. 2018;36(5):810-818. https://doi.org/10.1007/s10637-018-0571-3
24. Holstein SA, Hohl RJ. Isoprenoid biosynthetic pathway inhibition disrupts monoclonal protein secretion and induces the unfolded protein response pathway in multiple myeloma cells. *Leuk Res*. 2011;35(4):551-559. https://doi.org/10.1016/j.leukres.2010.08.008
25. Chhonker YS, Haney SL, Matthiesen RA, Wiemer DF, Holstein SA, Murry DJ. Quantitative determination of a potent geranylgeranyl diphosphate synthase inhibitor using LC-MS/MS: Derivatization and application. *J Pharm Biomed Anal*. 2018;153:22-28. https://doi.org/10.1016/j.jpba.2018.02.010
26. Chhonker YS, Haney SL, Bala V, Holstein SA, Murry DJ. Simultaneous quantitation of isoprenoid pyrophosphates in plasma and cancer cells using LC-MS/MS. *Molecules*. 2018;23(12):3275. https://doi.org/10.3390/molecules23123275
27. Savino S, Toscano A, Purgatorio R, et al. Novel bisphosphonates with antiresorptive effect in bone mineralization and osteoclastogenesis. *Eur J Med Chem*. 2018;158:184-200. https://doi.org/10.1016/j.ejmech.2018.08.044
28. Hsu H, Lacey DL, Dunstan CR, et al. Tumor necrosis factor receptor family member RANK mediates osteoclast differentiation and activation induced by osteoprotegerin ligand. *Proc Natl Acad Sci USA*. 1999;96(7):3540-3545. https://doi.org/10.1073/pnas.96.7.3540
29. Kong L, Smith W, Hao D. Overview of RAW264.7 for osteoclastogensis study: phenotype and stimuli. *J Cell Mol Med*. 2019;23(5):3077-3087. https://doi.org/10.1111/jcmm.14277
30. Collin-Osdoby P, Osdoby P. RANKL-mediated osteoclast formation from murine RAW 264.7 cells. *Methods Mol Biol*. 2012;816:187-202. https://doi.org/10.1007/978-1-61779-415-5_13
31. Minkin C. Bone acid phosphatase: tartrate-resistant acid phosphatase as a marker of osteoclast function. *Calcif Tissue Int*. 1982;34(1):285-290. https://doi.org/10.1007/bf02411252
32. Croke M, Ross FP, Korhonen M, Williams DA, Zou W, Teitelbaum SL. Rac deletion in osteoclasts causes severe osteopetrosis. *J Cell Sci*. 2011;124(22):3811-3821. https://doi.org/10.1242/jcs.086280
33. Wang Y, Lebowitz D, Sun C, Thang H, Grynpas MD, Glogauer M. Identifying the relative contributions of Rac1 and Rac2 to osteoclastogenesis. *J Bone Miner Res*. 2008;23(2):260-270. https://doi.org/10.1359/jbmr.071013
34. Ito Y, Teitelbaum SL, Zou W, et al. Cdc42 regulates bone modeling and remodeling in mice by modulating RANKL/M-CSF signaling and osteoclast polarization. *J Clin Invest*. 2010;120(6):1981-1993. https://doi.org/10.1172/jci39650
35. Touaitahuata H, Blangy A, Vives V. Modulation of osteoclast differentiation and bone resorption by Rho GTPases. *Small GTPases*. 2014;5(1):e28119. https://doi.org/10.4161/sgtp.28119
36. Zhao H, Ettala O, Väänänen HK. Intracellular membrane trafficking pathways in bone-resorbing osteoclasts revealed by cloning and subcellular localization studies of small GTP-binding Rab proteins. *Biochem Biophys Res Commun*. 2002;293(3):1060-1065. https://doi.org/10.1016/s0006-291x(02)00326-1
37. Sun Y, Büki KG, Ettala O, Vääräniemi JP, Väänänen HK. Possible role of direct Rac1-Rab7 interaction in ruffled border formation of osteoclasts. *J Biol Chem*. 2005;280(37):32356-32361. https://doi.org/10.1074/jbc.M414213200
38. Das BK, Minocha T, Kunika MD, et al. Molecular and functional mapping of Plekhm1-Rab7 interaction in osteoclasts. *JBMR Plus*. 2024;8(5). https://doi.org/10.1093/jbmrpl/ziae034
39. Saltel F, Destaing O, Bard F, Eichert D, Jurdic P. Apatite-mediated actin dynamics in resorbing osteoclasts. *Mol Biol Cell*. 2004;15(12):5231-5241. https://doi.org/10.1091/mbc.e04-06-0522
40. Duque G, Rivas D. Alendronate has an anabolic effect on bone through the differentiation of mesenchymal stem cells. *J Bone Miner Res*. 2007;22(10):1603-1611. https://doi.org/10.1359/jbmr.070701
41. Ebert R, Zeck S, Krug R, et al. Pulse treatment with zoledronic acid causes sustained commitment of bone marrow derived mesenchymal stem cells for osteogenic differentiation. *Bone*. 2009;44(5):858-864. https://doi.org/10.1016/j.bone.2009.01.009
42. Weivoda MM, Hohl RJ. The effects of direct inhibition of geranylgeranyl pyrophosphate synthase on osteoblast differentiation. *J Cell Biochem*. 2011;112(6):1506-1513. https://doi.org/10.1002/jcb.23087
43. Weivoda MM, Hohl RJ. Geranylgeranyl pyrophosphate stimulates PPARγ expression and adipogenesis through the inhibition of osteoblast differentiation. *Bone*. 2012;50(2):467-476. https://doi.org/10.1016/j.bone.2011.09.056
44. Yoshida T, Asanuma M, Grossmann L, et al. Geranylgeranyl-pyrophosphate (GGPP) synthase is down-regulated during differentiation of osteoblastic cell line MC3T3-E1. *FEBS Lett*. 2006;580(22):5203-5207. https://doi.org/10.1016/j.febslet.2006.08.060
45. Wiemer AJ, Yu JS, Lamb KM, Hohl RJ, Wiemer DF. Mono- and dialkyl isoprenoid bisphosphonates as geranylgeranyl diphosphate synthase inhibitors. *Bioorg Med Chem*. 2008;16(1):390-399. https://doi.org/10.1016/j.bmc.2007.09.029
46. Haider MT, Holen I, Dear TN, Hunter K, Brown HK. Modifying the osteoblastic niche with zoledronic acid in vivo-potential implications for breast cancer bone metastasis. *Bone*. 2014;66(100):240-250. https://doi.org/10.1016/j.bone.2014.06.023
47. Ebetino FH, Hogan AM, Sun S, et al. The relationship between the chemistry and biological activity of the bisphosphonates. *Bone*. 2011;49(1):20-33. https://doi.org/10.1016/j.bone.2011.03.774
48. Ebetino FH, Sun S, Cherian P, et al. Bisphosphonates: the role of chemistry in understanding their biological actions and structure-activity relationships, and new directions for their therapeutic use. *Bone*. 2022;156:116289. https://doi.org/10.1016/j.bone.2021.116289
49. Kavanagh KL, Guo K, Dunford JE, et al. The molecular mechanism of nitrogen-containing bisphosphonates as antiosteoporosis drugs. *Proc Natl Acad Sci USA*. 2006;103(20):7829-7834. https://doi.org/10.1073/pnas.0601643103

50. Nancollas GH, Tang R, Phipps RJ, et al. Novel insights into actions of bisphosphonates on bone: differences in interactions with hydroxyapatite. *Bone*. 2006;38(5):617-627. https://doi.org/10.1016/j.bone.2005.05.003
51. Jilka RL. The relevance of mouse models for investigating age-related bone loss in humans. *J Gerontol A Biol Sci Med Sci*. 2013;68(10):1209-1217. https://doi.org/10.1093/gerona/glt046
52. Zekri J, Mansour M, Karim SM. The anti-tumour effects of zoledronic acid. *J Bone Oncol*. 2014;3(1):25-35. https://doi.org/10.1016/j.jbo.2013.12.001
53. Lin Y, Villacanas MG, Zou H, et al. Calcium-bisphosphonate nanoparticle platform as a prolonged nanodrug and bone-targeted delivery system for bone diseases and cancers. *ACS Appl Bio Mater*. 2021;4(3):2490-2501. https://doi.org/10.1021/acsabm.0c01455
54. Li X, Valdes SA, Alzhrani RF, Hufnagel S, Hursting SD, Cui Z. Zoledronic acid-containing nanoparticles with minimum premature release show enhanced activity against extraskeletal tumor. *ACS Appl Mater Interfaces*. 2019;11(7):7311-7319. https://doi.org/10.1021/acsami.8b16588

JBMR Plus, 2025, 9, ziae133
https://doi.org/10.1093/jbmrpl/ziae133
Research Article